Beneficial Metabolic Effects of TREM2 in Obesity Are Uncoupled From Its Expression on Macrophages

Omar Sharif,[1,2,3,4] Julia Stefanie Brunner,[1,2,3,4] Ana Korosec,[1,2] Rui Martins,[1,2] Alexander Jais,[5] Berend Snijder,[2] Andrea Vogel,[3,4] Michael Caldera,[6] Anastasiya Hladik,[1,2] Karin Lakovits,[1,2] Simona Saluzzo,[1,2] Benedikta Boehm,[1,2] Anna-Dorothea Gorki,[1,2] Ildiko Mesteri,[7] Josefine Lindroos-Christensen,[5] Katharina Tillmann,[8] Dagmar Stoiber,[9,10] Jörg Menche,[2,6,11] Gernot Schabbauer,[3,4] Martin Bilban,[5] Giulio Superti-Furga,[2,9] Harald Esterbauer,[5] and Sylvia Knapp[1,2]

Diabetes 2021;70:2042–2057 | https://doi.org/10.2337/db20-0572

Obesity-induced white adipose tissue (WAT) hypertrophy is associated with elevated adipose tissue macrophage (ATM) content. Overexpression of the triggering receptor expressed on myeloid cells 2 (TREM2) reportedly increases adiposity, worsening health. Paradoxically, using insulin resistance, elevated fat mass, and hypercholesterolemia as hallmarks of unhealthy obesity, a recent report demonstrated that ATM-expressed TREM2 promoted health. Here, we identified that in mice, TREM2 deficiency aggravated diet-induced insulin resistance and hepatic steatosis independently of fat and cholesterol levels. Metabolomics linked TREM2 deficiency with elevated obesity-instigated serum ceramides that correlated with impaired insulin sensitivity. Remarkably, while inhibiting ceramide synthesis exerted no influences on TREM2-dependent ATM remodeling, inflammation, or lipid load, it restored insulin tolerance, reversing adipose hypertrophy and secondary hepatic steatosis of TREM2-deficient animals. Bone marrow transplantation experiments revealed unremarkable influences of immune cell–expressed TREM2 on health, instead demonstrating that WAT-intrinsic mechanisms impinging on sphingolipid metabolism dominate in the systemic protective effects of TREM2 on metabolic health.

Obesity and associated metabolic disorders like insulin resistance, type 2 diabetes, and hepatic steatosis constitute a major public health crisis. Obesity is characterized by excessive lipid accumulation in white adipose tissue

[1]Department of Medicine I, Laboratory of Infection Biology, Medical University of Vienna, Vienna, Austria
[2]Research Center for Molecular Medicine of the Austrian Academy of Sciences, Vienna, Austria
[3]Institute for Vascular Biology, Centre for Physiology and Pharmacology, Medical University Vienna, Vienna, Austria
[4]Christian Doppler Laboratory for Arginine Metabolism in Rheumatoid Arthritis and Multiple Sclerosis, Vienna, Austria
[5]Department of Laboratory Medicine, Medical University of Vienna, Vienna, Austria
[6]Department of Structural and Computational Biology, Max Perutz Laboratories, University of Vienna, Vienna, Austria
[7]Institute of Pathology, Überlingen, Germany
[8]Center of Biomedical Research, Medical University of Vienna, Vienna, Austria
[9]Institute of Pharmacology, Center of Physiology and Pharmacology, Medical University of Vienna, Vienna, Austria
[10]Division of Pharmacology, Department of Pharmacology, Physiology and Microbiology, Karl Landsteiner University of Health Sciences, Krems, Austria
[11]Faculty of Mathematics, University of Vienna, Vienna, Austria

Corresponding authors: Omar Sharif, omar.sharif@meduniwien.ac.at, and Sylvia Knapp, sylvia.knapp@meduniwien.ac

Received 5 June 2020 and accepted 19 February 2021

This article contains supplementary material online at https://doi.org/10.2337/figshare.14074550.

J.S.B. is currently affiliated with Cell Biology Program, Sloan Kettering Institute, Memorial Sloan Kettering Cancer Center, New York, NY.

A.K. is currently affiliated with the Skin and Endothelium Research Division, Department of Dermatology, Medical University of Vienna, Vienna, Austria.

R.M. is currently affiliated with Instituto Gulbenkian de Ciência, Oeiras, Portugal.

A.J. is currently affiliated with the Helmholtz Institute for Metabolic, Obesity and Vascular Research, Leipzig, Germany.

B.S. is currently affiliated with the Department of Biology, Institute of Molecular Systems Biology, ETH Zurich, Zurich, Switzerland.

S.S. is currently affiliated with the Department of Dermatology, Medical University of Vienna, Vienna, Austria.

J.L.-C. is currently affiliated with Novo Nordisk, Søborg, Denmark.

See accompanying article p. 1926.

(WAT), pathological WAT expansion, adipocyte hypertrophy, and WAT immune cell infiltration, with adipose tissue macrophages (ATMs) constituting a substantial fraction of this cell infiltrate (1).

ATM numbers increase through monocyte recruitment into adipose, occurring partly through MCP-1/C-C chemokine receptor type 2 (2,3). Although in diet-induced obesity (DIO) ATMs were proposed to promote low-grade adipose inflammation contributing to insulin resistance (4,5), observations have indicated that extensive ATM heterogeneity, suggesting, in DIO, increases in ATM number rather than activation, may be responsible for low-grade adipose inflammation (6–8). F4/80$^+$CD11b$^+$CD11c$^-$ (FB) ATMs represent resident macrophages, while F4/80$^+$CD11b$^+$CD11c$^+$ (FBC) ATMs represent newly recruited cells rich in lysosomal markers that also express CD9 (4,6,9). Single-cell RNA sequencing studies have corroborated the concept of obesity-instigated dynamic ATM remodeling and heterogeneity, further indicating that CD9-expressing ATMs are circulation derived and possess a transcriptional signature associated with lipid metabolism and phagocytosis (8,9). Together, ATMs respond to their lipid-rich environment and fulfill their main function of clearing up dying adipocytes and preventing peripheral lipid spillover that are the consequences of DIO-instigated exhausted adipose expansion (1,10,11). Numerous studies have indicated that ectopic lipid storage is associated with impaired insulin signaling and resistance. Participating lipid species include various ceramides and complex sphingolipids, like glucosylceramides, lactosylceramide, sphingomyelin and sialic acid–containing glycosphingolipids such as ganglioside GM3 (12–14).

The triggering receptor on myeloid cell 2 (TREM2) regulates osteoclastogenesis and microglial responses, and genetic variants of TREM2 are risk factors for Alzheimer disease (15–17). Consistent with studies demonstrating TREM2 binding to various lipids, including sphingomyelin, phosphatidylcholine, and cardiolipin (18,19), TREM2-deficient microglia exhibit lipid metabolism defects (20). Mice globally overexpressing TREM2 exhibit impaired insulin sensitivity following caloric excess, an effect attributed to increases in body adiposity, suggesting that TREM2 exerts detrimental effects on metabolic health (21). In contrast, a recent report demonstrated that mice globally genetically lacking TREM2 also exhibit weight gain, aggravated insulin resistance, and glucose intolerance. This study assigned a critical role for immune cell–expressed TREM2 to these effects, particularly suggesting that lipid-associated TREM2 and CD9-expressing ATMs prevent DIO-instigated adipose hypertrophy and loss of metabolic homeostasis (8).

Here, we identified that during DIO, TREM2 deficiency was associated with attenuated FBC ATMs that progressively led to selective ATM loss, which coincided with accelerated secondary hepatic steatosis and sphingolipid-mediated toxicity. Bone marrow (BM) transplantation showed that although macrophage/immune cell–expressed TREM2 restrained adipose hypertrophy, this was uncoupled from the protective effects of TREM2 on metabolic health.

RESEARCH DESIGN AND METHODS

Animals

All procedures were conducted in compliance with protocols approved by the Medical University of Vienna and the Austrian Ministry of Sciences under project number BMWF-66.009/0276-II/3b/2013. *Trem2*$^{-/-}$ mice backcrossed onto a 98% C57BL/6 background were previously described (22). Wild-type (WT) C57BL/6J and B6.SJL-*Ptprc*^{a}*Pepc*^{b}/BoyCrl (herein CD45.1) mice were purchased from Charles River Laboratories (#CRL:632, #CRL:494). All mice were bred at the Medical University of Vienna and housed under specific-pathogen–free conditions, with temperatures ranging from 21 to 23°C in cages (five mice per cage) with microisolator tops and a 12-h light cycle (7:00 A.M.–7:00 P.M.). Unless otherwise indicated, 6-week-old male age-matched mice were used. Dietary interventions started at 6 weeks of age using a diet that contained 60% calories of fat (high-fat diet [HFD]) (#D12492; Research Diets).

Human Subjects

Visceral adipose biopsies from individuals who were lean (n = 23), obese insulin resistant (obIR) who clearly exhibited elevated insulin resistance (HOMA of insulin resistance [HOMA-IR] ≥5) (n = 31), and obese insulin sensitive (obIS) who showed no signs of systemic insulin resistance (i.e., HOMA-IR ≤2) (n = 29) were obtained under informed consent as previously described (23).

BM Transplantation

BM transplantation was performed as previously described (24). Whole BM from WT C57BL/6J and *Trem2*$^{-/-}$ donor mice was prepared by flushing the tibia and femur with sterile RPMI medium. Two million cells were injected retro-orbitally into lethally irradiated (9 Gy) 6-week-old recipient WT and *Trem2*$^{-/-}$ male mice under anesthesia. After a 6-week recovery period (25) during which the mice were placed on a normal chow diet (ND), mice were administered an HFD for the indicated times. As a control for chimerism, some mice received CD45.1 marrow, and chimerism was determined using flow cytometry. The population of CD11b$^+$CD45.1$^+$ cells within the blood was >99%, demonstrating successful transplantation.

Sphingolipid Blockage During DIO

Myriocin was administered as previously described, with some minor modifications (26,27). Eight weeks after DIO, mice were injected three times weekly with saline control or myriocin (#M1177; Sigma-Aldrich) at a dose of 0.5 mg/kg and maintained on an HFD for the indicated times.

Glucose and Insulin Tolerance tests

Following an overnight fast, mice were administered 20% glucose (1 g/kg) by oral gavage, and blood samples for glucose and insulin measurements were collected from the tail vein at the indicated times. Insulin tolerance was assessed after a 2-h fast by intraperitoneal administration of human regular insulin (0.75 units/kg). Glycemia was assessed using an Accu-Chek glucometer in combination with Accu-Chek GO test strips (#05182913; Roche). Following insulin tolerance tests, mice were allowed to recover for 4–6 days, after which oral glucose tolerance was measured.

Statistical Analysis

Data are expressed as mean ± SEM. Statistical significance in two-group comparisons was assessed with an unpaired Student *t* test. When indicated, a Mann-Whitney *U* test was used for analysis of nonparametric data. Insulin tolerance test and oral glucose tolerance test data were analyzed using a two-way ANOVA followed by Bonferroni posttest with both time and group as sources of variation. For multivariable comparisons, we performed a one-way ANOVA followed by Tukey multiple comparison test. Results were analyzed with GraphPad Prism 8 software, and $P < 0.05$ was regarded as statistically significant.

Data and Resource Availability

The data sets generated and analyzed during this study are available from the corresponding authors upon reasonable request. Additional methods are described in the Supplementary Material.

RESULTS

TREM2 Is Upregulated in Visceral Adipose During Obesity in Mice and Humans

To explore the role of TREM2 during DIO, we first fed C57BL/6J mice a 60% HFD for 13 weeks and observed elevated *Trem2* in heart, kidney, and liver relative to animals fed ND (Fig. 1*A*). Notably, *Trem2* expression increased in all tested metabolically unhealthy mouse visceral WAT depots as opposed to healthy subcutaneous fat (Fig. 1*B*) (28,29). To examine whether DIO affected *Trem2* expression on infiltrating FBC ATMs (4,5) or mature adipocytes (MA), we isolated both MA and the stromal vascular fraction from the epididymal WAT (eWAT) of HFD-fed animals and subsequently positively selected the stromal vascular fraction for $CD11c^+$ cells and examined *Trem2* levels in both cell types. While F4/80 and adiponectin were selectively expressed on ATMs or MA, *Trem2* was detected on both cell types (Fig. 1*C*). Immunohistochemistry confirmed strong TREM2 expression within inflammatory crown-like structures that were clearly increased during DIO (Fig. 1*D*). To test whether increases in obesity-induced visceral adipose *Trem2* expression were conserved, we measured *Trem2* levels in a previously published cohort of clinically obese (BMI >30 kg/m^2) and age-matched individuals who were obIR (HOMA-IR ≥5), obIS (HOMA-IR ≤2), and lean (23). *Trem2* was elevated in the visceral adipose of individuals who were obIR versus obIS and lean (Fig. 1*E*). Thus, DIO results in conserved increases in *Trem2* expression within the visceral adipose of mice and humans and is associated with insulin resistance.

Loss of TREM2 Aggravates Metabolic Disease

To address the role of TREM2 in metabolic disease, we fed $Trem2^{-/-}$ mice an HFD for 13 weeks and assessed their metabolic health compared with WT C57BL/6J controls. $Trem2^{-/-}$ mice clearly exhibited impaired insulin sensitivity and glucose tolerance (Fig. 2*A–C*). These effects were independent of weight, and there were no differences in fat mass in both the subcutaneous and the visceral depots between genotypes (Fig. 2*D* and *E*). Time course experiments in independent cohorts of mice corroborated no differences in weight gain between genotypes, showing that $Trem2^{-/-}$ animals became insulin insensitive versus controls 8 weeks post-HFD, which progressively worsened over time (Supplementary Fig. 1*A* and *B*). Importantly, $Trem2^{-/-}$ mice exhibited normal insulin tolerance relative to WT animals in the naive and ND state, demonstrating that metabolic stress induced by HFD feeding was required for TREM2 to influence metabolic health (Supplementary Fig. 1*A*). Considering that single-cell RNA sequencing studies imply that the TREM2 pathway represents a conserved macrophage response for the detection of pathogenic lipids across multiple tissues (8) and an interrelationship between insulin resistance and Alzheimer disease is suggested (30), of which TREM2 genetic variants are a risk factor (17), we next let both genotypes age to 1 year and examined insulin tolerance. These experiments confirmed the unremarkable effects of TREM2 on insulin sensitivity in the context of ND, even upon aging (Supplementary Fig. 1*C* and *D*). The decreased insulin sensitivity of $Trem2^{-/-}$ animals 13 weeks post-HFD was independent of changes in serum cholesterol and triglycerides (Supplementary Fig. 2*A*). In line, we observed no differences in liver triglycerides, steatosis, and serum indicators of hepatotoxicity, including ALT and AST, 13 weeks post-HFD (Supplementary Fig. 2*B–D*). To shed light on the physiological mechanisms whereby TREM2 affected insulin resistance, we next performed indirect calorimetry on weight-matched obese mice but did not observe differences in energy expenditure or activity between genotypes (Fig. 2*F–H*). Together, these data largely support findings indicating that in DIO-instigated insulin resistance, TREM2 exerts protective effects (8,21). However, given that global overexpression of TREM2 (21) as well as TREM2 deficiency (8) was reported to promote weight gain upon HFD, our data indicate that loss of metabolic homeostasis in obese TREM2-deficient mice did not correlate with increases in fat mass.

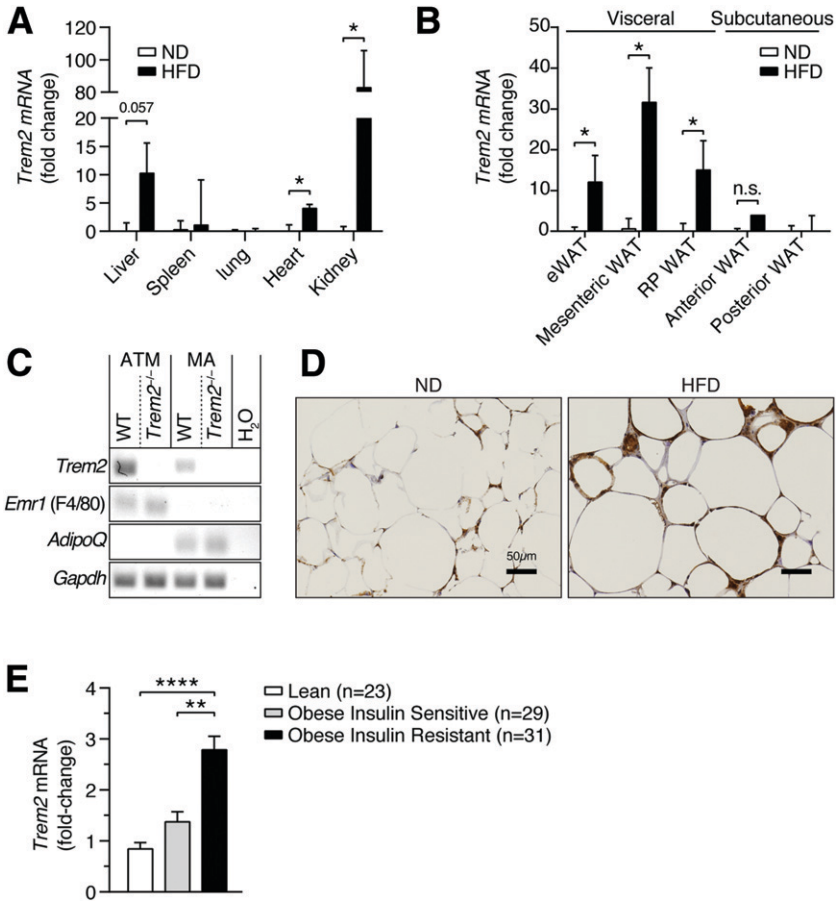

Figure 1—Conserved visceral adipose upregulation of TREM2 in obesity. *A*: *Trem2* expression in organs 13 weeks post-HFD. *B*: *Trem2* expression in visceral and subcutaneous adipose depots 13 weeks post-HFD. *C*: *Trem2* expression in ATMs and MA. *D*: Immunohistochemistry of eWAT depicting TREM2 13 weeks post-HFD. *E*: *Trem2* expression in human visceral adipose biopsies obtained from individuals who were obIS and obIR. Bar graph bar data are mean ± SEM ($n = 4$ per diet). Statistical analysis was performed with Mann-Whitney *U* test (*A* and *B*) or two-way ANOVA followed by Bonferroni posttest (*E*). *$P < 0.05$, **$P < 0.01$, ****$P < 0.0001$. RP, retroperitoneal.

Elevated Adipose Hypertrophy in Obese TREM2-Deficient Animals Is Associated With Remodeling of ATM Populations

We next monitored visceral adipose hypertrophy in both sets of obese animals. The eWAT of *Trem2*$^{-/-}$ mice contained larger hypertrophic adipocytes versus controls, suggesting that TREM2 prevented pathological adipose expansion during HFD feeding (Fig. 3*A* and *B*). Pathological WAT expansion of obese mice is associated with WAT hypoxia and activation of the oxygen-sensitive transcription factor hypoxia-inducible factor 1α (HIF-1α), which heterodimerizes with HIF-1β to activate hypoxia-related transcription (1,31). Evaluating eWAT transcript levels of *Hif-1*α, *Hif-1*β, and other well-established components of the hypoxia pathway (31) demonstrated unremarkable differences between HFD-fed genotypes (Supplementary Fig. 3*A*). Further, proapoptotic *Bax* was unaltered and antiapoptotic *Bcl-2* levels elevated in hypertrophic *Trem2*$^{-/-}$ eWAT, suggesting that the elevated hypertrophy was not associated with augmented apoptosis (Supplementary Fig. 3*A*). Confirmatory and consistent with published observations indicating that significant adipocyte apoptosis in eWAT peaks between 16 and 20 weeks of HFD feeding (32), we could not detect any active caspase-3 in 13-week HFD-fed animals (Supplementary Fig. 3*B* and *C*). Together these observations suggest that the larger hypertrophic adipocytes of *Trem2*$^{-/-}$ animals are disconnected from elevated hypoxia and apoptosis.

We next examined whether there were differences in visceral eWAT ATM profiles between obese genotypes. Circulation-derived FBC ATMs comprise the majority of increased ATM content in obesity (4,6,33). CD206 is a marker for alternatively activated ATMs that is also robustly expressed by FB (CD11c^{-}) ATMs in the lean state (34). Monitoring visceral ATM content demonstrated that while obesity was associated with marked overall ATM expansion and recruitment, there were no differences between genotypes (Fig. 3*C* and *D*). Consistent with reports that DIO instigated preferential increases in FBC over FB ATMs (4,6,33), HFD feeding led to a shift in ATM populations, with an increased ratio of FBCs versus CD206-

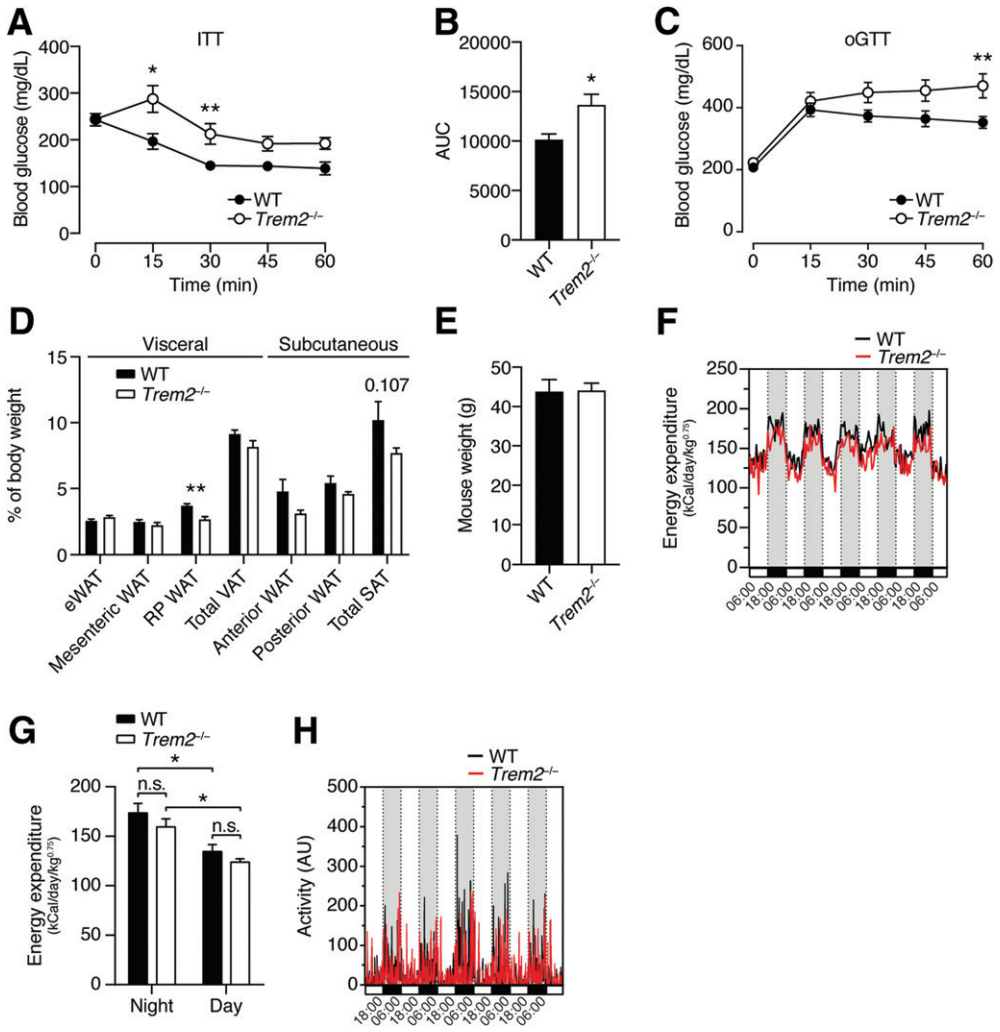

Figure 2—TREM2 deficiency aggravates obesity-induced insulin resistance. *A*: Insulin tolerance test (ITT) of WT and *Trem2*$^{-/-}$ mice 13 weeks post-HFD ($n = 8$ per genotype). *B*: Area under the curve (AUC) of panel *A*. *C*: Oral glucose tolerance test (oGTT) of WT and *Trem2*$^{-/-}$ mice 13 weeks post-HFD ($n = 8$ per genotype). *D*: Adipose weights 13 weeks post-HFD of animals in panel *C*. *E*: Mouse weights 13 weeks post-HFD of animals in panels *C* and *D*. *F–H*: Energy expenditure and activity of control and *Trem2*$^{-/-}$ mice 13 weeks post-HFD ($n = 4$ per genotype). Data are mean ± SEM and are pooled for panels *A–E* from two independent experiments. Statistical analysis was performed with two-way ANOVA followed by Bonferroni posttest (*A* and *C*), Student *t* test (*B* and *D*), or one-way ANOVA followed by Tukey posttest (*G*). *$P < 0.05$, **$P < 0.01$. AU, arbitrary unit; RP, retroperitoneal; SAT, subcutaneous adipose tissue; VAT, visceral adipose tissue.

expressing FBs that was dramatically attenuated upon TREM2 deficiency (Fig. 3*E* and Supplementary Fig. 4*A*). Indeed, the ATM compartment of obese *Trem2*$^{-/-}$ mice exhibited substantial remodeling with decreased FBCs and elevated levels of CD206-expressing FBs and FBCs versus control animals (Fig. 3*F* and *G*). Altogether, these data suggest that although the aggravated metabolic disease upon loss of TREM2 is associated with augmented adipocyte hypertrophy, the ATM signature within this hypertrophic adipose is skewed, incompletely advancing to the HFD state observed in controls.

Protective Effects of TREM2 on Metabolic Health in Obesity Are Linked to Sphingolipids

We next used mass spectrometry to determine which metabolic stressors were associated with the aggravated insulin resistance of *Trem2*$^{-/-}$ animals. We quantified 429 serum metabolites, including various lipid species like sphingolipids, sphingomyelin, acylcarnitines, and glycerophospholipids, in both sets of animals under both dietary conditions. We chose these metabolites because they are associated with insulin resistance (13,35–37), and glycerophospholipids, including phosphatidylcholines and phosphatidylglycerols, are reported to activate TREM2 signaling (19). Targeted metabolomics of serum from control and *Trem2*$^{-/-}$ mice on an ND or HFD for 14 weeks indicated that the metabolic effect of TREM2 deficiency was similar to that of HFD feeding (correlation of significantly altered metabolites is 0.56, $P < 2 \times 10^{-11}$) and that long-chain ceramides (C16:0, C18:0, C20:0), selected acylcarnitines (C18:0, C18:1, C18:2), and sphingomyelin (C22:3) were significantly upregulated following both HFD

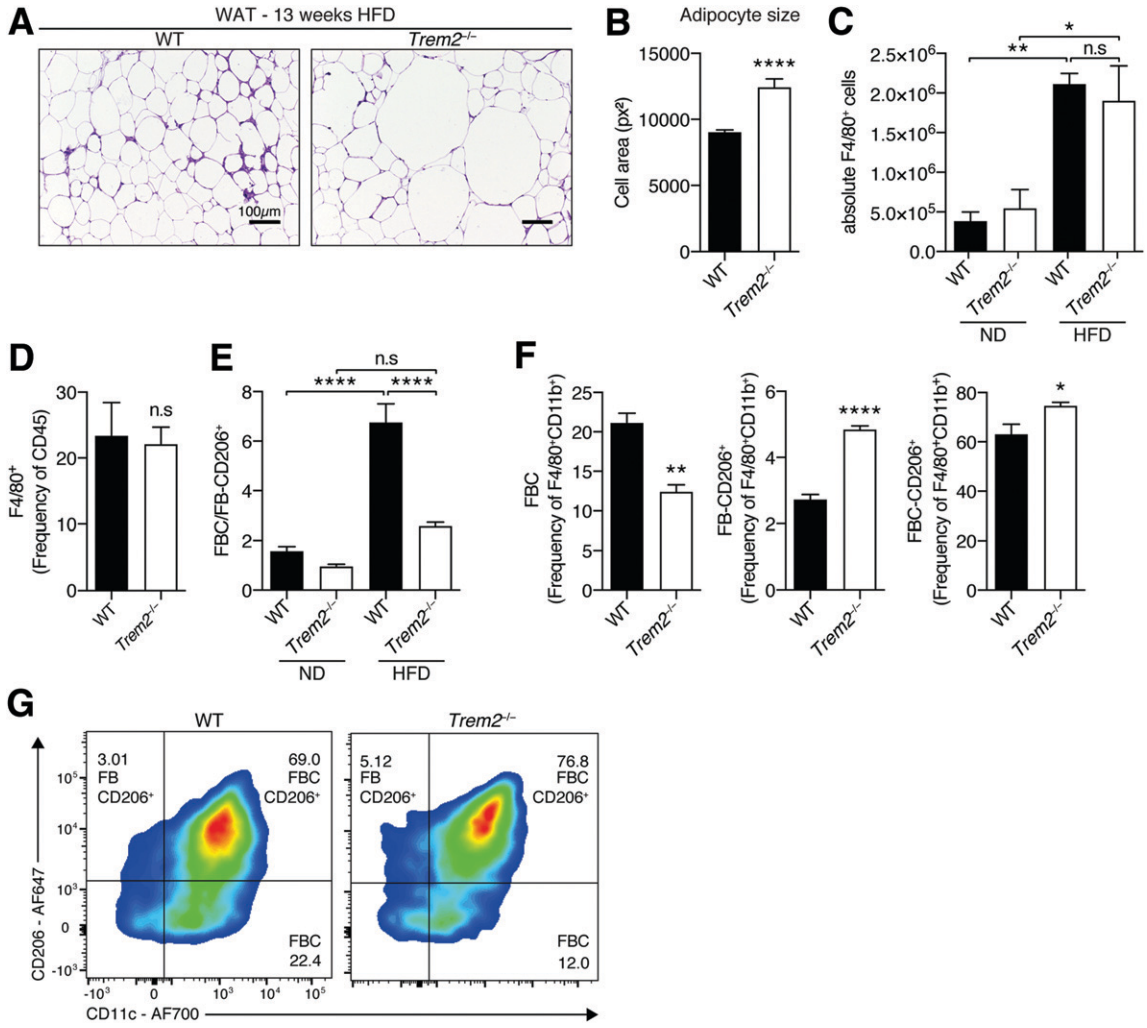

Figure 3—Elevated adipose hypertrophy of obese TREM2-deficient animals is associated with ATM remodeling. *A*: Representative hematoxylin-eosin staining of eWAT of WT and *Trem2*$^{-/-}$ mice 13 weeks post-HFD ($n = 8$ mice per genotype). *B*: Quantification of adipocyte cell size of WT and *Trem2*$^{-/-}$ mice 13 weeks post-HFD ($n = 8$ mice per genotype, and data correspond to size quantification of 3,492 WT and 2,103 *Trem-2*$^{-/-}$ adipocytes). *C*: Absolute macrophage content (defined as viable CD45$^+$F4/80$^+$CD11b$^+$ cells) in eWAT of both genotypes of animals following 13 weeks of feeding under both dietary conditions ($n = 4$ mice per condition). *D*: Percentage of macrophages (defined as viable CD45$^+$F4/80$^+$ cells) in eWAT of both genotypes of animals 13 weeks post-HFD ($n = 4$ mice per genotype). *E*: Ratio of FBC (viable CD45$^+$F4/80$^+$CD11b$^+$CD11c$^+$CD206$^-$ cells) vs. FB206 (viable CD45$^+$F4/80$^+$CD11b$^+$CD206$^+$ cells) in eWAT of both genotypes of animals following 13 weeks of feeding under both dietary conditions ($n = 4$ mice per genotype). *F*: Percentage within the parent FB population of CD206$^+$, CD11c$^+$, and CD206$^+$CD11c$^+$ ATMs in both genotypes of obese animals 13 weeks post-HFD ($n = 4$ mice per genotype). *G*: Representative flow cytometry plots of panel *F*. Bar graph data are mean ± SEM and are pooled for panels *A* and *B* from two independent experiments. Data in panels *E*–*G* are representative of two independent experiments. Statistical analysis was performed with Student *t* test (*B*, *D*, and *F*) or one-way ANOVA followed by Tukey posttest (*C* and *E*). *$P < 0.05$, **$P < 0.01$, ****$P < 0.0001$. px^2, square pixels.

feeding and TREM2 ablation (Fig. 4*A*). Systematically comparing metabolite levels in mice with low- and high-glucose levels upon 45 min of insulin treatment revealed gradual and stepwise relationships between the relative abundance of these same metabolites and insulin resistance, with levels of ceramides (C16:0, C18:0, C20:0) and sphingomyelin (C22:3) being highest in HFD-fed *Trem2*$^{-/-}$ mice (Fig. 4*B* and Supplementary Fig. 5*A*). Correlations between abundance of these metabolites and glycemia were rapid and evident 15 min postinsulin treatment (Supplementary Fig. 5*B*). Because ceramides are potent lipotoxic mediators in obesity, which attenuate insulin signaling in part by inactivating the kinase AKT (12,38), we assessed hepatic AKT activity after intraperitoneal administration of insulin to both groups of HFD-fed animals. Loss of TREM2 was associated with substantially decreased insulin-stimulated liver AKT phosphorylation, indicating that following 13 weeks of HFD feeding, TREM2 deficiency elicited body-wide changes in insulin sensitivity and that sphingolipids might be causally linked (Fig. 4*C*).

To demonstrate that altered sphingolipid metabolism was crucial to the insulin resistance of metabolically stressed *Trem2*$^{-/-}$ animals, we next blocked sphingolipid

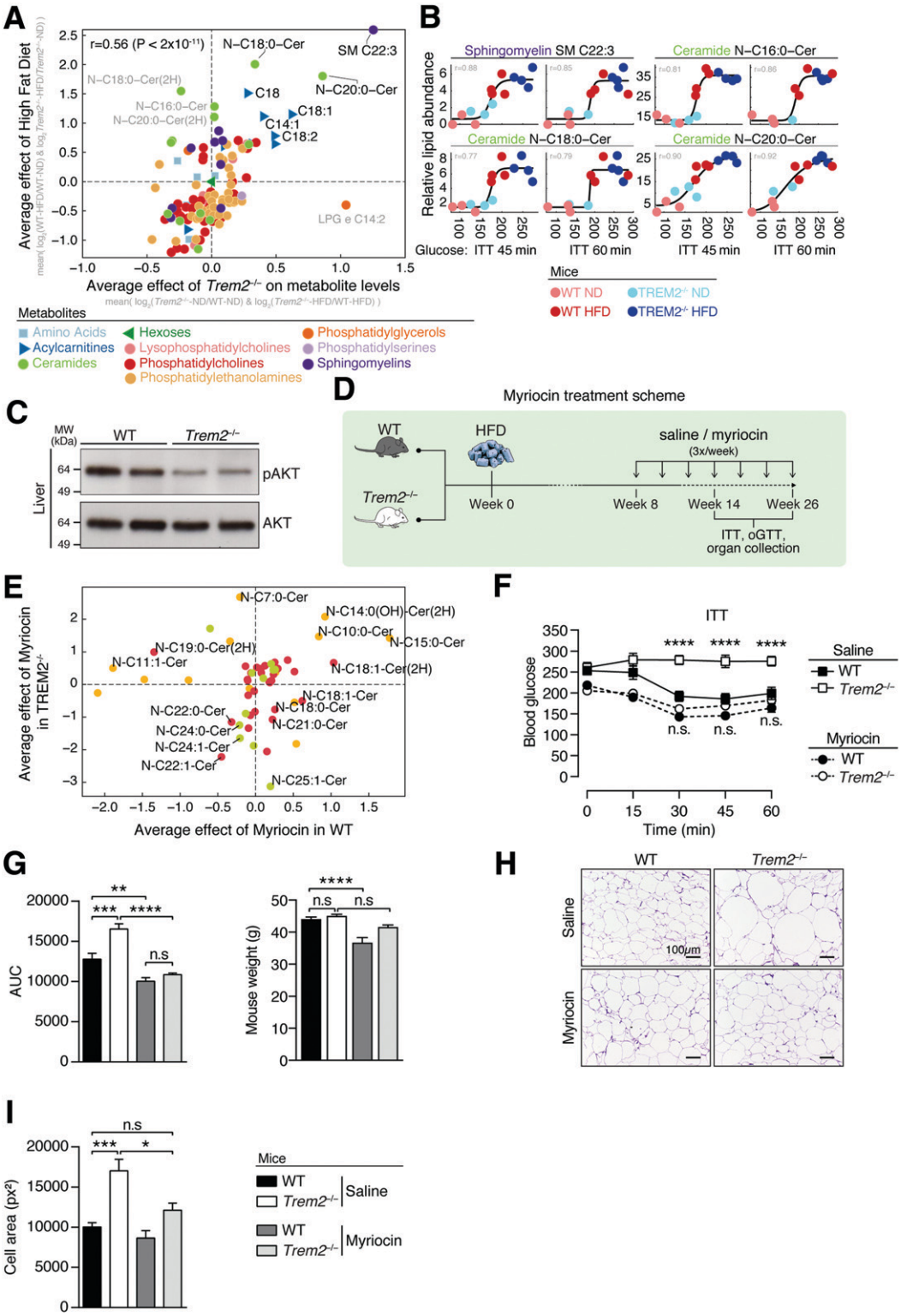

Figure 4— Metabolic stress is required for the protective effects of TREM2, which are linked to elevated sphingolipids levels. *A*: Log_2 fold change (FC) in metabolite abundance for *Trem2*$^{-/-}$ over WT mice averaged over both dietary conditions compared with log_2(FC) metabolite levels of HFD over ND averaged over both genetic groups (n = 3 or 4 mice per genotype following 14 weeks of ND or HFD, respectively). *B*: Glucose levels (x-axis) vs. relative abundance of selected lipids (y-axis) following 45 and 60 min of insulin challenge. Dots represent mice, colored as indicated in the key. *C*: Activation of liver AKT signaling 5 min post–insulin injection in both genotypes fed an HFD for 13 weeks. *D*: Scheme for sphingolipid blockage. WT or *Trem2*$^{-/-}$ mice were placed on an HFD for 13 or 26 weeks. Eight weeks post-DIO, mice were injected three times weekly with saline control or myriocin at a dose of 0.5 mg/kg and maintained on an HFD. *E*: Log_2FC in average abundance of short-, long-, and ultra-long-chain ceramides for both genotypes of myriocin-treated animals compared with saline controls (n = 4 mice per condition 26 weeks post-HFD). *F*: Insulin tolerance test (ITT) of both genotypes of mice in the context of

synthesis at a time post-DIO when *Trem2*$^{-/-}$ animals first become insulin resistant versus controls (i.e., 8 weeks following HFD) (Supplementary Fig. 1*A*) and subsequently examined animals post-DIO (Fig. 4*D*). We treated both genotypes with myriocin, a specific inhibitor of serine palmitoyl-transferase, the rate-limiting enzyme of de novo ceramide synthesis that converts palmitoyl-CoA and serine into ceramides (12,26,27). Targeted serum metabolomics reproduced that long-chain ceramides (C16:0–C24:0) were particularly upregulated by the HFD feeding regimen (Supplementary Fig. 6*A*). Notably, in both genotypes, myriocin treatment during HFD feeding led to an upregulation in short-chain ceramides (<C16:0) and downregulation of long- and ultra-long ceramides (>C16:0), an effect that was particularly prominent in TREM2-deficient animals (Supplementary Fig. 6*B*). Short-chain ceramides upregulated by myriocin in both genotypes included C10:0 and C15:0, while long- and ultra-long ceramides downregulated included C22:1 and C24:0. Ceramides particularly affected by myriocin in *Trem2*$^{-/-}$ animals included C18:0, C21:0, and C25:1 (Fig. 4*E*). Together, these data indicate that myriocin negatively affects the serum levels of metabolically detrimental long- and ultra-long-chain ceramide species (26,36,39), suggesting that it might improve insulin sensitivity. Indeed, *Trem2*$^{-/-}$ animals treated with saline control were insulin resistant compared with WT mice, and myriocin treatment completely reversed this impaired insulin sensitivity, with both effects independent of weight (Fig. 4*F* and *G*). Further, myriocin treatment of *Trem2*$^{-/-}$ animals decreased metabolic stress-induced adipocyte enlargement to levels of control animals, demonstrating the contribution of sphingolipids to visceral adipose morphology and expansion (Fig. 4*H* and *I*). These data assign a strong contribution of metabolic stress-induced sphingolipid and long-chain ceramide synthesis (>C16:0) to the elevated insulin resistance and adipose hypertrophy of TREM2-deficient animals.

We next examined the impact of myriocin treatment on ATM numbers, remodeling, and inflammation. Sphingolipid blockage exerted both unremarkable effects on ATM content and remodeling because obese *Trem2*$^{-/-}$ animals treated with myriocin still exhibited decreased FBCs and elevated levels of CD206-expressing FBs compared with control mice (Fig. 5*A*–*C*). To evaluate the impacts of myriocin on ATM inflammation within the eWAT of both obese genotypes 13 weeks post-HFD, using F4/80 and CD11b antibodies, we performed flow-assisted cell sorting on a pool of FB-ATMs that express CD11c, CD206, or both markers (Supplementary Fig. 4A). Consistent with the incomplete ATM remodeling of *Trem2*$^{-/-}$ animals versus controls, reproducibly elevated expression of canonical markers of alternative macrophage (M2) activation, *Fizz1* and *Ym1* (40), was apparent in *Trem2*$^{-/-}$ ATMs isolated from different obese animals (Fig. 5*D*). However, suggesting that TREM2 does not alter ATM-mediated inflammation, there were no reproducible decreases in markers of classical M1 activation (*iNOS*) (40) or differences in proinflammatory cytokine expression between ATM genotypes. Importantly, sphingolipid blockage exerted no influences herein (Fig. 5*D*).

Since lipid-associated TREM2-expressing ATMs were recently reported to prevent DIO-instigated adipose hypertrophy and loss of metabolic homeostasis (8), in the same cohort of animals, we evaluated impacts of TREM2 on ATM-mediated lipid uptake and the effects of myriocin herein. Although, as previously observed, there were no differences in overall ATM expansion between genotypes, 4,4-difluoro-1,3,5,7,8-pentamethyl-4-bora-3a,4a-diaza-s-indacene (BODIPY) staining (BODIPY 493/503) revealed fewer lipid-laden *Trem2*$^{-/-}$ ATMs, confirming published data that ATM-expressed TREM2 is associated with lipid uptake in obesity (8) (Figs. 3*D* and 5*E* and *F*). While there was a slight tendency ($P = 0.0892$) that myriocin treatment increased the attenuated lipid load of *Trem2*$^{-/-}$ ATMs, this was not statistically significant. Collectively, these data suggest that the effects of sphingolipids on adipose hypertrophy and metabolic health are uncoupled from TREM2-dependent shifts in ATM remodeling, inflammation, and lipid load.

TREM2 Exerts Protective Effects in Secondary Liver Steatosis That Are Associated With Specific Defects in ATM Content and Sphingolipids

Insulin resistance is often accompanied by hepatic steatosis. Because *Trem2*$^{-/-}$ mice were more insulin resistant compared with controls 13–14 weeks post-DIO, despite no differences in hepatic steatosis (Figs. 2 and 4 and Supplementary Fig. 2), we next hypothesized that prolonged HFD feeding might unleash a secondary steatotic phenotype in these animals. An extended 26-week HFD regimen led to striking insulin resistance with liver morphology and scoring of liver steatosis by an experienced pathologist, indicating that *Trem2*$^{-/-}$ animals exhibited larger and more steatotic livers as opposed to controls (Fig. 6*A*–*C*). Further, akin to 13 weeks of HFD feeding (Fig. 3*E*), prolonged obesity was associated with a decreased ratio of FBCs versus CD206-expressing FBs (Fig. 6*D*). The visceral adipose of TREM2-deficient animals exhibited ATM loss, suggesting that decreased circulation-derived FBCs upon TREM2 deficiency impacted ATM content during prolonged 26 weeks of HFD feeding compared with controls

sphingolipid blockage 13 weeks post-HFD (n = 8–9 mice per condition). *G*: Area under the curve (AUC) and mouse weights of data in panel *F*. *H*: Representative hematoxylin-eosin staining of eWAT 13 weeks post-HFD of animals in panels *F* and *G* (n = 8–9 mice per condition). *I*: Quantification of adipocyte cell size in panel *H*. Data are mean ± SEM. Statistical analysis was performed with two-way ANOVA followed by Bonferroni posttest (*F*) or one-way ANOVA followed by Tukey posttest (*G* and *I*). *$P < 0.05$, **$P < 0.01$, ***$P < 0.001$, ****$P < 0.0001$. MW, molecular weight; oGTT, oral glucose tolerance test; px^2, square pixels.

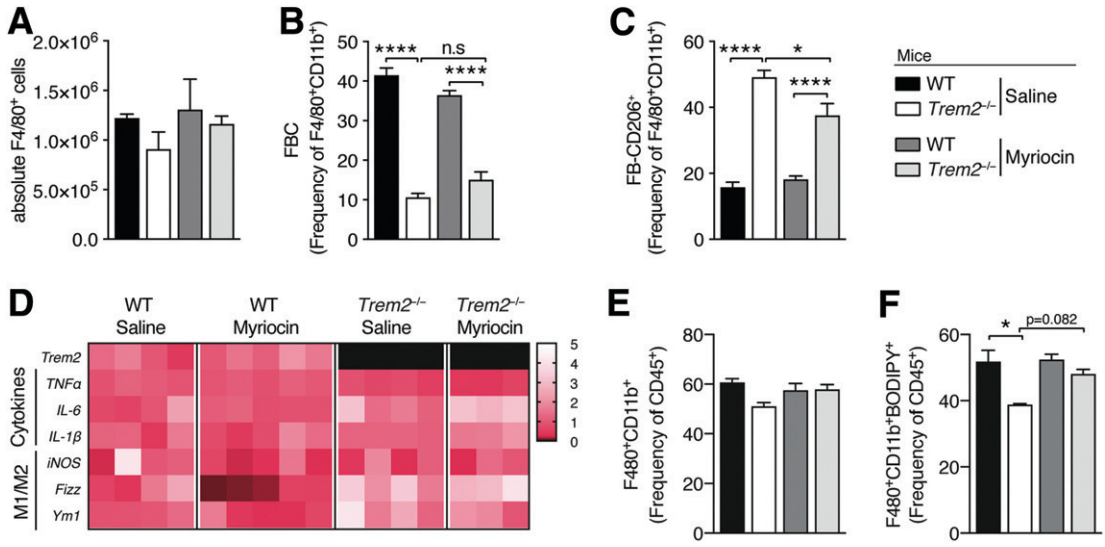

Figure 5—Sphingolipid blockage exerts no effects on the ATM compartment of *Trem2*$^{-/-}$ mice. *A*: Absolute eWAT macrophage content of both genotypes of animals (defined as viable CD45$^+$F4/80$^+$CD11b$^+$ cells) in the context of sphingolipid blockage 13 weeks post-HFD ($n = 5$ mice per condition). *B* and *C*: Percentage within the parent FB population of CD206$^+$ and CD11c$^+$ ATMs in both genotypes of obese animals 13 weeks post HFD in the context of sphingolipid blockage ($n = 5$ mice per condition). *D*: ATM-mediated polarization and inflammation from flow-assisted cell-sorted viable CD45$^+$CD3$^-$F4/80$^+$CD11b$^+$ cells of both genotypes of animals in the context of sphingolipid blockage 13 weeks post-HFD ($n = 3$–5 mice per condition). Data are fold change relative to WT saline animals. *E*: Percentage of macrophages (defined as viable CD45$^+$F4/80$^+$CD11b$^+$ cells) in eWAT of both genotypes of animals in the context of sphingolipid blockage 13 weeks post-HFD ($n = 3$–5 mice per condition). *F*: Percentage of BODIPY$^+$ macrophages (defined as viable BODIPY$^+$CD45$^+$F4/80$^+$CD11b$^+$ cells) in eWAT of both genotypes of animals in the context of sphingolipid blockage 13 weeks post-HFD ($n = 3$–5 mice per condition). Data are mean ± SEM. Statistical analysis was performed with one-way ANOVA followed by Tukey posttest (*A–C*, *E*, and *F*). $^*P < 0.05$, $^{****}P < 0.0001$.

(Fig. 6*E* and *F*). These lower macrophage numbers were specific for fat macrophages and independent of differences in circulating or inflammatory monocytes because there were no differences in hepatic macrophage content or white blood cell counts between obese genotypes (Supplementary Fig. 4*B–E* and Fig. 6*G*). Hypothesizing that upon prolonged HFD feeding, attenuated chemotactic signals for ATM recruitment and expansion within the visceral adipose environment of TREM2-deficient animals might be responsible, we next prepared MA from both sets of obese genotypes and generated adipocyte-conditioned media (ACM). Despite comparable protein content in both genotypes, ACM derived from adipocytes collected from 26-week HFD-fed TREM2-deficient animals exhibited significantly reduced MCP-1 amounts that in turn generated lower migratory responses of macrophages compared with ACM from 26-week HFD-fed control animals (Fig. 6*H* and *I*). Together, these data indicate that signals derived from the adipose environment contribute to ATM content. This observation is consistent with adipocytes being significant sources of MCP-1 (2) and suggest influences of TREM2 herein.

Because metabolic stress-induced sphingolipid synthesis was critical for the elevated insulin resistance of TREM2-deficient animals, we next hypothesized that inhibition of de novo ceramide synthesis might reverse the enhanced hepatic steatosis of these animals. Histology and liver morphology revealed that sphingolipid blockage during prolonged 26-week HFD feeding ameliorated the accelerated secondary hepatic steatosis of *Trem2*$^{-/-}$ animals to control levels (Fig. 6*J* and *K*). These data firmly place metabolic stress-induced sphingolipid synthesis at the crux of the protective effects of TREM2 during metabolic health.

Nonhematopoietic-Expressed TREM2 Influences Metabolic Health

To unveil the contribution of TREM2 expressed on hematopoietic versus nonhematopoietic cells to the insulin resistance of *Trem2*$^{-/-}$ mice, we next performed BM transplantation to generate four groups of mice: WT (WT>WT), *Trem2*$^{-/-}$ (*Trem2*$^{-/-}$>*Trem2*$^{-/-}$) or chimeric mice-WT mice with *Trem2*$^{-/-}$ BM (*Trem2*$^{-/-}$>WT), and *Trem2*$^{-/-}$ mice transplanted with WT BM (WT>*Trem2*$^{-/-}$) (Fig. 7*A*). Surprisingly, following 13 weeks of HFD, recipient *Trem2*$^{-/-}$ mice transplanted with either genotype of BM displayed more pronounced insulin resistance and glucose intolerance compared with WT or WT chimeric (*Trem2*$^{-/-}$>WT) controls (Fig. 7*B–E*). Examining insulin tolerance 26 weeks post-HFD feeding confirmed these effects, demonstrating that they were independent of weight

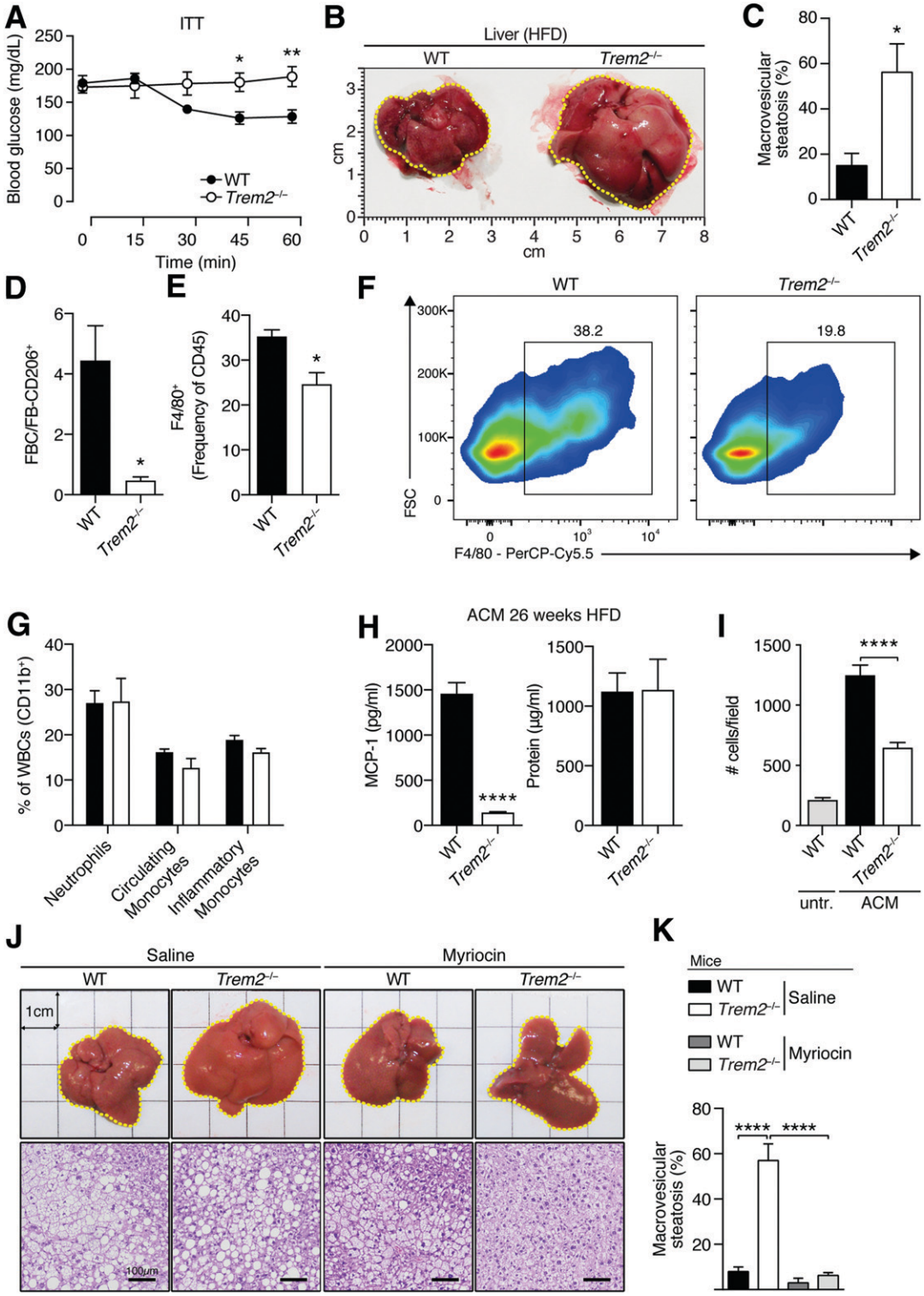

Figure 6—TREM2 exerts protective effects in sphingolipid-mediated secondary liver steatosis associated with specific defects in visceral ATM content. *A*: Insulin tolerance test (ITT) 26 weeks post-HFD ($n = 4$ per genotype). *B*: Liver size 26 weeks post-HFD ($n = 4$ per genotype). *C*: Liver steatosis 26 weeks post-HFD ($n = 4$ per genotype). *D*: Ratio of FBC (viable $CD45^+F4/80^+CD11b^+CD11c^+$ cells) vs. FB206 (viable $CD45^+F4/80^+CD11b^+CD206^+$ cells) in eWAT of both genotypes of animals 26 weeks post-HFD ($n = 4$ mice per genotype). *E*: Percentage of macrophages (viable $CD45^+Ly6G^-F4/80^+$) in eWAT 26 weeks post-HFD ($n = 4$ per genotype). *F*: Representative flow cytometry plots of panel *E*. *G*: Percentage of white blood cells (WBCs) evaluated using flow cytometry 26 weeks post-HFD ($n = 4$ per genotype). *H*: MCP-1 levels and protein content in ACM derived from WT and *Trem2*$^{-/-}$ mice 26 weeks post-HFD ($n = 5$ mice per genotype). *I*: Migration levels of BM macrophages induced by ACM in panel *H* ($n = 4$ per condition). *J*: Representative liver morphology and hematoxylin-eosin staining 26 weeks post-HFD in the context of sphingolipid blockage ($n = 4$–5 mice per genotype). *K*: Liver steatosis 26 weeks post-HFD in the context of sphingolipid blockage ($n = 4$–5 mice per genotype). Data are mean ± SEM. Data in panels *A*–*F*, *H*, and *I* are

differences (Supplementary Fig. 7*A* and *B*). Together, these data demonstrate a major contribution of nonhematopoietic-expressed TREM2 to metabolic health.

In evaluating TREM2 and F4/80 levels in eWAT, visualization of F4/80 using alkaline phosphatase together with permanent red chromogen and TREM2 with horseradish peroxidase coupled to diaminobenzidine as a substrate, resulting in brown color, revealed significant colocalization in WT>WT animals. While both genotypes transplanted with *Trem2*$^{-/-}$ BM (*Trem2*$^{-/-}$>WT or *Trem2*$^{-/-}$>*Trem2*$^{-/-}$) exhibited only red color in the crown-like structures, *Trem2*$^{-/-}$ animals transplanted with WT BM displayed brownish color, with some areas of colocalization. These data confirm TREM2 loss in ATMs in animals transplanted with *Trem2*$^{-/-}$ BM and are consistent with data showing that the majority of ATMs in obesity are circulation derived (8,33,41). Examining eWAT F4/80 transcript levels revealed decreased levels in recipient *Trem2*$^{-/-}$ mice transplanted with either genotype of BM compared with WT control mice (WT>WT), supporting our observations that chemotactic signals leading to ATM recruitment and expansion were attenuated within visceral adipose upon TREM2 deficiency (Supplementary Fig. 8*A* and Fig. 6*H* and *I*). More definitive evidence was provided by experiments where we transplanted WT CD45.1 BM into both WT and *Trem2*$^{-/-}$ animals and evaluated blood monocyte and ATM levels using flow cytometry. While both genotypes of animals exhibited a similar reconstitution of CD45.1-derived blood monocytes 26 weeks post-HFD, the frequency of circulation-derived CD45.1 ATMs were significantly lower in TREM2-deficient mice (Supplementary Fig. 8*B–D*). Together, these data confirm the importance of signals derived from the visceral adipose of obese animals and a role for TREM2 in governing ATM content.

Importantly, while transplantation of WT mice with *Trem2*$^{-/-}$ BM (*Trem2*$^{-/-}$>WT) exerted no effects on metabolic disease, it significantly increased adipose hypertrophy (Fig. 7*F* and *G*). A more pronounced effect was observed upon transplantation of WT BM in *Trem2*$^{-/-}$ mice (WT>*Trem2*$^{-/-}$), which despite exerting unremarkable effects on metabolic health, were completely able to reverse the elevated adipose hypertrophy of TREM2-deficient animals (Fig. 7*F* and *G*). Thus, although in obesity hematopoietic/macrophage-expressed TREM2 restrains adipose hypertrophy, it exerts no influences on metabolic health.

The Elevated Hepatic Steatosis of TREM2-Deficient Animals Is Linked to Visceral Adipose Tissue–Derived Ceramide Lipotoxicity

We next examined the cell type–specific contributions of TREM2 to hepatic steatosis. Importantly, the metabolic improvements elicited by nonhematopoietic-expressed TREM2 were systemic. Both liver morphology and scoring of liver steatosis revealed more severe steatosis in recipient *Trem2*$^{-/-}$ animals, regardless of genotype of transplanted BM, compared with WT recipient mice (Fig. 8*A* and *B*). These effects were confirmed by increased oil red O staining and elevated serum hepatotoxicity markers in recipient *Trem2*$^{-/-}$ mice (Fig. 8*A* and *C*) and were independent of changes in serum triglyceride and cholesterol levels (Supplementary Fig. 7*C* and *D*). Interestingly, assessing eWAT architecture using whole-mount microscopy and BODIPY labeling following prolonged HFD feeding revealed uniform staining of lipid droplets in adipose of WT mice, while in both groups of recipient *Trem2*$^{-/-}$ mice, adipose architecture was markedly different, with areas displaying more intense staining (Fig. 8*A*). Noting this and that the elevated hepatic steatosis of *Trem2*$^{-/-}$ animals was linked to ceramide levels (Fig. 6*J* and *K*), we next evaluated visceral eWAT adipose ceramide levels in the HFD-fed BM-transplanted animals. Remarkably, compared with recipient WT mice, diverse short- and long-chain ceramide species were reproducibly elevated in the eWAT of recipient *Trem2*$^{-/-}$ animals, regardless of genotype of transplanted BM (Fig. 8*D* and Supplementary Fig. 9).

Because adipose tissue is a significant ceramide source impacting hepatic steatosis during HFD feeding (39,40), using immunohistochemistry with a ceramide-detecting antibody that does not cross react with sphingomyelin, cholesterol, or other phospholipids, we next evaluated hepatic ceramide levels. Consistent with elevated ceramide eWAT presence, recipient *Trem2*$^{-/-}$ animals displayed augmented hepatic ceramide levels, which was particularly prominent in steatotic and ballooned hepatocytes (Fig. 8*A*). Thus, prolonged obesity in TREM2-deficient mice is associated with lipotoxic effects that are linked to elevated visceral adipose ceramide production.

To further examine potential contributions of TREM2 to adipose-derived signals and systemic metabolism, we next asked whether the elevated sphingolipid and long-chain ceramide species present in serum of HFD-fed *Trem2*$^{-/-}$ mice versus WT controls (Fig. 4 and Supplementary Fig. 6A) were linked to adiponectin levels, which exert beneficial metabolic effects through sphingolipid metabolism and catabolism of cellular ceramide (42). In line with the contributions of nonhematopoietic-expressed TREM2 to metabolic health and the elevated ceramide species found in eWAT of *Trem2*$^{-/-}$ animals, we found decreased adiponectin levels in recipient *Trem2*$^{-/-}$ mice transplanted with either genotype of BM (Fig. 8*E*). These data further strengthen the importance of

representative of two independent experiments. Statistical analysis was performed with two-way ANOVA followed by Bonferroni posttest (*A*), Student *t* test (*C–E* and *H*), or one-way ANOVA followed by Tukey posttest (*I* and *K*). *$P < 0.05$, **$P < 0.01$, ****$P < 0.0001$. untr., untreated.

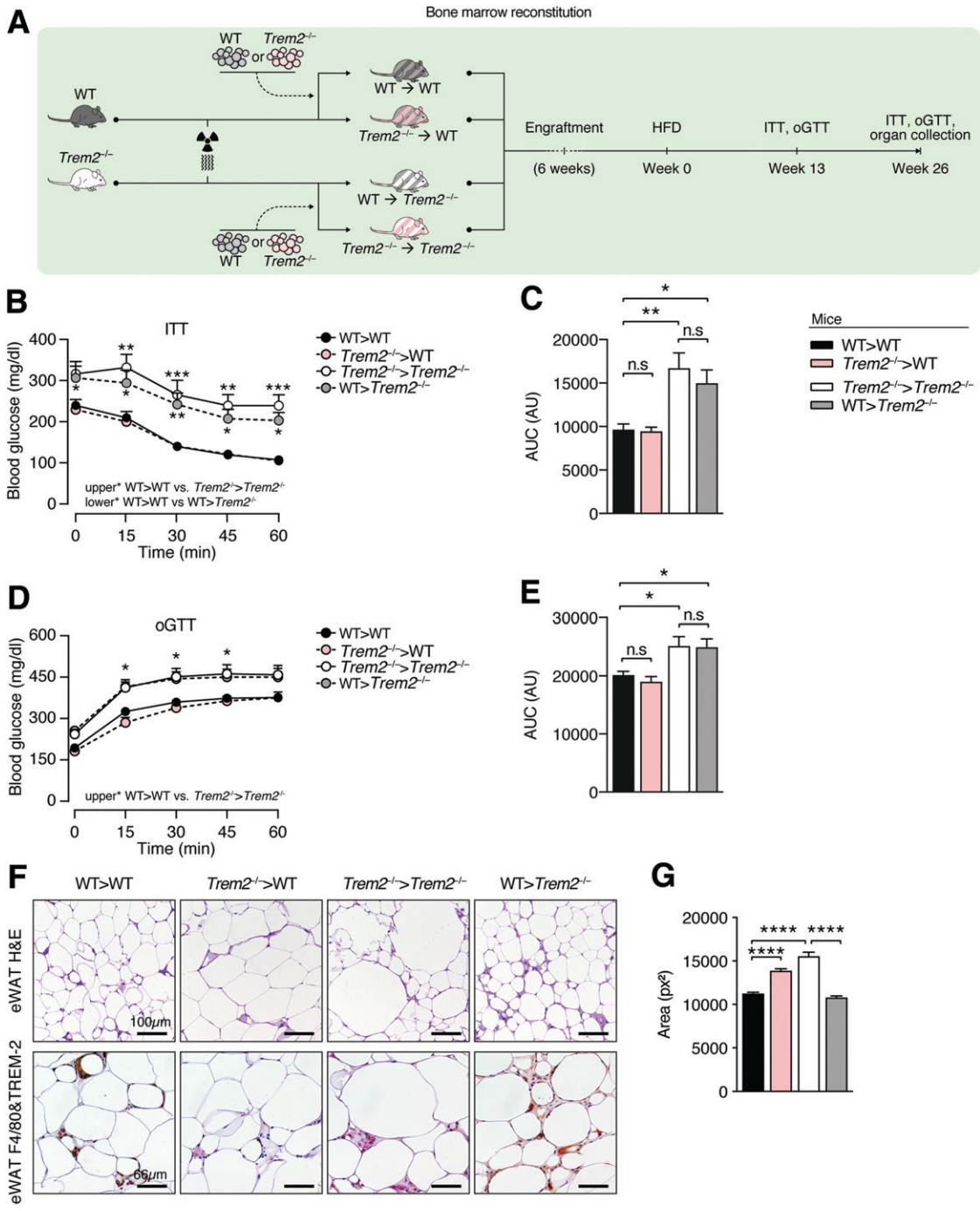

Figure 7—Uncoupling of effects of hematopoietic-expressed TREM2 on adipose hypertrophy and metabolic health. *A*: Scheme for BM transplantation studies. WT or *Trem2*$^{-/-}$ mice were lethally irradiated and transplanted with either WT or *Trem2*$^{-/-}$ BM to generate four groups of mice: WT>WT, *Trem2*$^{-/-}$>*Trem2*$^{-/-}$ or *Trem2*$^{-/-}$>WT, and WT>*Trem2*$^{-/-}$. Posttransplant mice were maintained on an ND for 6 weeks, following which DIO was instigated. *B*: Insulin tolerance test (ITT) 13 weeks post-HFD. *C*: Area under the curve (AUC) of data in panel *B*. *D*: Oral glucose tolerance test (oGTT) 13 weeks post-HFD. *E*: AUC of data in panel *D*. *F*: Representative hematoxylin-eosin (H&E), TREM2, and F4/80 staining of eWAT of BM-transplanted mice 26 weeks post-HFD. *G*: Quantification of adipocyte cell size in H&E staining from panel *F*. Data correspond to size quantification of 3,868, 3,147, 3,198, and 4,412 adipocytes in WT>WT, *Trem2*$^{-/-}$>WT, *Trem2*$^{-/-}$>*Trem2*$^{-/-}$, and WT>*Trem2*$^{-/-}$ mice, respectively. Data are mean ± SEM and are pooled from two independent experiments (n = 10–13 mice per genotype). Statistical analysis was performed with two-way ANOVA followed by Bonferroni posttest (*B* and *D*) or one-way ANOVA followed by Tukey posttest (*C*, *E*, and *G*). *$P < 0.05$, **$P < 0.01$, ***$P < 0.01$, ****$P < 0.0001$. AU, arbitrary unit; px^2, square pixels.

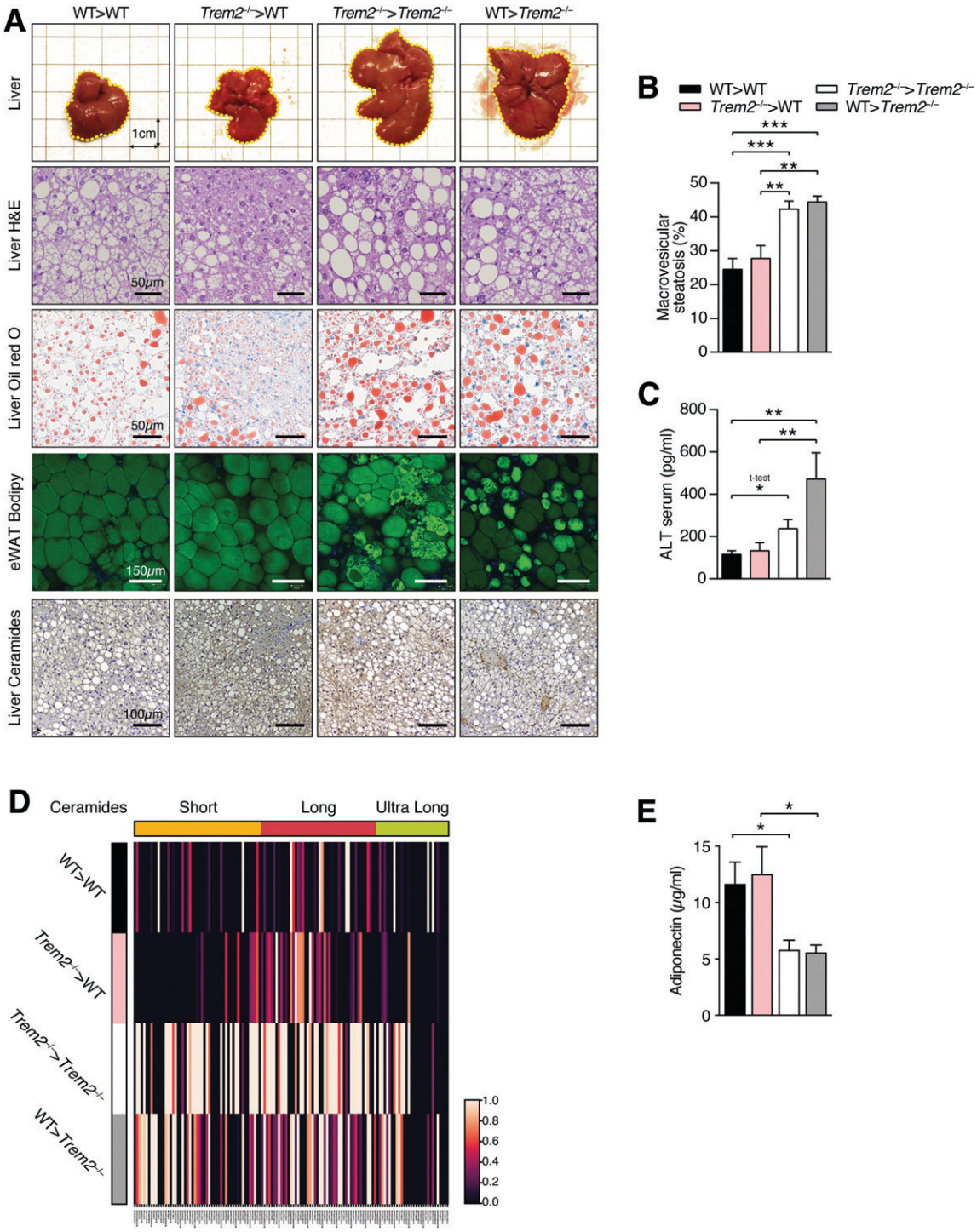

Figure 8—Effects of TREM2 on hepatic steatosis are linked to nonhematopoietic tissue and elevated adipose ceramide levels. *A*: Liver aspects and stainings of representative liver sections (hematoxylin-eosin [H&E], oil red O, ceramide) and representative whole mount of eWAT of BM-transplanted mice 26 weeks post-HFD. *B*: Liver steatosis in groups of BM-transplanted mice 26 weeks post-HFD. *C*: Serum levels of ALT 26 weeks post-HFD. *D*: Average abundance of short-, long-, and ultra-long-chain ceramide species in eWAT of BM-transplanted mice 26 weeks post-HFD. Individual ceramide abundances scaled between 0 (minimum) and 1 (maximum) ($n = 4$ mice per genotype). *E*: Serum adiponectin levels 26 weeks post-HFD. Data are mean ± SEM (*B*, *C*, and *E*) and pooled from two independent experiments ($n = 10$–13 mice per genotype). Statistical analysis was performed with one-way ANOVA followed by Tukey posttest (*B*, *C*, and *E*). *$P < 0.05$, **$P < 0.01$, ***$P < 0.01$.

nonhematopoietic TREM2 in protecting against insulin resistance and hepatic steatosis, supporting the notion that adipose tissue–derived signals might be responsible for the aggravated metabolic disease and ceramide-instigated lipotoxicity of TREM2-deficient animals.

DISCUSSION

Here, we show that during obesity, *Trem2* expression increases in unhealthy visceral adipose in mice and humans (28,29), and in humans, augmented *Trem2* was highest in individuals who are obIR, indicating this receptor's importance in metabolic health. Although elevated visceral adipose *Trem2* in obesity is likely due to increases in ATM content (4,33), in contrast to a recent report demonstrating a crucial role for immune cell–expressed TREM2 in protecting against insulin resistance and glucose intolerance (8), the BM transplantation experiments herein argue that hematopoietic-expressed TREM2 is dispensable for these obesity-triggered health complications. In contrast to the aforementioned report, we further demonstrate that the aggravated metabolic disease of TREM2-deficient animals is not associated with hematopoietic cell–expressed TREM2-instigated increases in cholesterol and body adiposity (8). Moreover, we show that lipotoxic signals triggered by HFD feeding arising from metabolically stressed TREM2-deficient adipose are sufficient to exacerbate metabolic disease, independent of macrophage and adipose mass influences.

Obesity-instigated adipose hypertrophy is associated with both adipocyte death and increases in ATMs that are proposed to phagocytose dying adipocytes in crown-like structures and scavenge residual lipid droplets (1,10,11). Recent work using single-cell RNA sequencing demonstrated that TREM2 is required for the formation of lipid-associated macrophage (LAM) cell-rich crown-like structures and assigned LAMs as $CD9^{+}CD63^{+}TREM2^{+}$ cells rich in lysosomal markers exhibiting a transcriptional signature associated with lipid metabolism and phagocytosis (8). Other work showed that CD9-expressing ATMs also express CD11c and assigned a critical function for FBCs that are circulation derived in lipid metabolism (4,6,9). Although we could not reproduce data demonstrating a protective effect for hematopoietic-expressed TREM2 in metabolic disease, consistent with observations that LAM accumulation is substantially reduced in HFD fed $Trem2^{-/-}$ mice (8), we could demonstrate decreased FBCs upon TREM2 deficiency in obesity. Notably, because transplantation of WT mice with $Trem2^{-/-}$ BM significantly increased adipose hypertrophy, we could directly demonstrate that in obesity, hematopoietic/likely macrophage–expressed TREM2 regulates adipose hypertrophy. In this regard, it is notable that multiple studies focusing on the brain, where TREM2 is an established player, have demonstrated the critical role of TREM2 in the uptake of apoptotic cells and amyloid plaques (43). Although in obesity ATM-expressed TREM2 might be important for the uptake of dying adipocytes, depletion of CD206-expressing ATMs attenuates adipose hypertrophy by increasing adipocyte progenitor proliferation and differentiation (44), suggesting potential involvement of shifts toward increased CD206 expression in eWAT of WT animals transplanted with $Trem2^{-/-}$ BM. However, our data indicate that decreases in ATMs stemming from circulation-derived FBCs in obese TREM2-deficient mice per se likely play a more important role in the elevated adipose hypertrophy of these animals. Concordantly, transplantation of $Trem2^{-/-}$ mice with WT BM could completely reverse the elevated hypertrophy of HFD-fed $Trem2^{-/-}$ animals. Interestingly, HFD-fed $Trem2^{-/-}$ mice transplanted with $Trem2^{-/-}$ BM displayed the most adipose hypertrophy, suggesting additional requirements for TREM2 expression on adipocytes where TREM2 is described to be important for adipocyte differentiation (21). The exact functions and interplay of TREM2 expression on adipose versus macrophages in the hypertrophy phenotype will be interesting areas for future investigation.

Notably, TREM2 only affected insulin sensitivity following HFD feeding. TREM2-deficient mice fed an ND or aged mice lacking TREM2 in the context of ND feeding exhibited unremarkable differences in insulin sensitivity relative to controls, indicating that a trigger is required for TREM2 to confer a health benefit in obesity. Herein, both HFD feeding and TREM2 deficiency exhibited commonalities on dyslipidemia, with both increasing serum levels of long-chain ceramides. Cellular ceramide is formed in various ways (12), and reducing the condensation of serine with palmitoyl-CoA and, hence, production of 3-ketosphinganine during metabolic stress, using myriocin (12,26,27), abolished all detrimental effects of TREM2 deficiency in obesity, indicating that de novo ceramide production is connected to TREM2's influence. These effects were independent of body adiposity but connected to adipose ceramide production. Accordingly, independent of weight, depletion of ceramides through transgenic overexpression of acid ceramidase in adipose of obese animals causes decreased systemic ceramide levels and improved insulin sensitivity (45). Lowering adipose ceramides by genetically targeting adipose-specific *Sptlc2* or through overexpression of adipose-specific acid ceramidase in obese animals also improves hepatic steatosis, implying that adipose and liver shuttle sphingolipids or that both tissues function as sinks for circulating ceramides during HFD feeding (45,46). Our data are consistent with an adipose-liver sphingolipid cross talk hypothesis and demonstrate the contribution of TREM2 therein. In line, early in obesity, as opposed to controls, $Trem2^{-/-}$ animals exhibited no differences in hepatic steatosis, yet pronounced decreases in insulin-stimulated liver AKT phosphorylation, that correlated with adipose hypertrophy and increased systemic long-chain ceramides that inhibit insulin signaling (26,36). Prolonged HFD feeding of TREM2-deficient animals caused extensive hepatic steatosis

connected to elevated hepatic ceramide presence, which coincided with visceral adipose ceramide production and dysfunction, indicating that ceramides stored within adipose were spilled into the circulation and deposited in the liver. Decreasing de novo ceramide synthesis in TREM2-deficient animals reversed elevated hepatic steatosis to control levels, which was preceded in timing by attenuated adipose hypertrophy during HFD feeding. However, decreasing de novo ceramide synthesis exerted no influence on the ATM remodeling observed in TREM2-deficient animals, indicating that these two phenomena are uncoupled.

Further, there were no effects of sphingolipid blockage on ATM-mediated inflammation, which did not differ between HFD-fed genotypes, indicating that the incomplete ATM remodeling of TREM2-deficient animals early in obesity does not impact classical M1 ATM activation. Consistently, ATMs, especially FBC or CD9-expressing ATMs, are described to adopt a unique metabolically activated phenotype, which is not classically M1, in response to their lipid-rich environment (6,7). In this regard, although sphingolipid blockage did not statistically increase the reduced lipid load in ATMs of obese *Trem2*$^{-/-}$ animals, there was a tendency, suggesting an involvement for WAT-derived lipids and ceramides in the attenuated neutral lipid content of ATMs from obese *Trem2*$^{-/-}$ animals.

While our study does not support a role for TREM2 expression on macrophages being related to TREM2's beneficial metabolic effects in obesity, it strongly suggests that the effects of TREM2 on metabolic disease are linked to sphingolipid homeostasis and metabolic stress within adipose. Nonetheless, we acknowledge the limitations. First, the exact contribution of TREM2 expression on MA to metabolic health would require conditional loss-of-function approaches. The TREM2-deficient animals used in this study and those by Jaitin et al. (8) and Turnbull et al. (22), which demonstrated a protective role of immune cells expressed in metabolic health primarily through BM transplantation, possess a deletion in a portion of the transmembrane and cytoplasmic domains encoded by exons 3 and 4 of *Trem2*. To our knowledge, no conditional TREM2 mouse exists that possesses *loxP* sites targeting *Trem2* at this region. Moving forward, generating these animals and crossing them to mice expressing the Cre recombinase under the adiponectin promoter would be important. Second, although akin to Jaitin et al. versus controls we could demonstrate incomplete ATM remodeling within TREM2-deficient hypertrophic adipose as well as decreased insulin sensitivity and glucose tolerance, contrasting results between BM transplantation studies with TREM2-deficient BM might be impacted by differences in microbiota and mouse house-specific facility factors.

Ending hypothetically, >25 years ago, the bone cysts in human TREM2 deficiency (Nasu Hakola disease) were described to consist of membranous and lamellar structures composed of phospholipids and triglycerides (47). Further, some disease cases exhibited sphingolipid species within the brain cortex and white matter–like C16:0 and C18:0 fatty acid sulfatides, cerebrosides, and gangliosides (48). More recently, TREM2 binding to various lipids was demonstrated (18,19). TREM2-deficient microglia exhibit lipid metabolism defects (20), providing a mechanistic explanation for why rare variants of TREM2 promote Alzheimer disease (17), which intriguingly is believed to be a form of brain insulin resistance coined "type 3 diabetes" (30). Together with our data, these published observations hint at the intriguing possibility that by sensing nutrients and binding elevated adipose-derived or -circulating sphingolipids during obesity, TREM2 and possibly adipose-specific TREM2 may act as a sink, promoting healthy function during nutrient excess. Our work also suggests that examining the interplay among TREM2, sphingolipid synthesis, and brain insulin resistance in the context of Alzheimer disease models might uncover hidden secrets on how TREM2 affects late-onset dementia.

Acknowledgments. The authors thank the staff of the animal facility at the Medical University of Vienna.

Funding. This work was funded by the Austrian Science Fund (FWF P25801 and FWF P31568 to O.S.) and the special research program Immunothrombosis of the Austrian Science Fund (F5410-B21 to S.K.).

Duality of Interest. No potential conflicts of interest relevant to this article were reported.

Author Contributions. O.S. designed the study and overall research plan and performed and analyzed data for the majority of the experiments. O.S. and S.K. conceived the project. J.S.B., A.K., A.V., A.H., K.L., S.S., B.B., A.D.-G., J.L.-C., D.S., G.S., and M.B. helped with the experiments. R.M. analyzed adipocyte cell size and performed experiments. A.J. and H.E. collected and analyzed human data, helped with metabolic cages, and contributed to the project design. B.S., M.C., J.M., and G.S.-F. analyzed lipidomics data. I.M. analyzed liver steatosis. K.T. contributed to mouse husbandry/veterinary care. O.S. and S.K. wrote the manuscript and all authors read, revised and approved the final manuscript. O.S. and S.K. are guarantors of this work and, as such, had full access to all the data in the study and take responsibility for the integrity of the data and the accuracy of the data analysis.

References

1. Rutkowski JM, Stern JH, Scherer PE. The cell biology of fat expansion. J Cell Biol 2015;208:501–512

2. Kanda H, Tateya S, Tamori Y, et al. MCP-1 contributes to macrophage infiltration into adipose tissue, insulin resistance, and hepatic steatosis in obesity. J Clin Invest 2006;116:1494–1505

3. Kamei N, Tobe K, Suzuki R, et al. Overexpression of monocyte chemoattractant protein-1 in adipose tissues causes macrophage recruitment and insulin resistance. J Biol Chem 2006;281:26602–26614

4. Lumeng CN, Bodzin JL, Saltiel AR. Obesity induces a phenotypic switch in adipose tissue macrophage polarization. J Clin Invest 2007;117:175–184

5. Patsouris D, Li PP, Thapar D, Chapman J, Olefsky JM, Neels JG. Ablation of CD11c-positive cells normalizes insulin sensitivity in obese insulin resistant animals. Cell Metab 2008;8:301–309

6. Xu X, Grijalva A, Skowronski A, van Eijk M, Serlie MJ, Ferrante AW Jr. Obesity activates a program of lysosomal-dependent lipid metabolism in adipose tissue macrophages independently of classic activation. Cell Metab 2013;18:816–830

7. Kratz M, Coats BR, Hisert KB, et al. Metabolic dysfunction drives a mechanistically distinct proinflammatory phenotype in adipose tissue macrophages. Cell Metab 2014;20:614–625
8. Jaitin DA, Adlung L, Thaiss CA, et al. Lipid-associated macrophages control metabolic homeostasis in a Trem2-dependent manner. Cell 2019;178: 686–698.e14
9. Hill DA, Lim HW, Kim YH, et al. Distinct macrophage populations direct inflammatory versus physiological changes in adipose tissue. Proc Natl Acad Sci U S A 2018;115:E5096–E5105
10. Coats BR, Schoenfelt KQ, Barbosa-Lorenzi VC, et al. Metabolically activated adipose tissue macrophages perform detrimental and beneficial functions during diet-induced obesity. Cell Rep 2017;20:3149–3161
11. Cinti S, Mitchell G, Barbatelli G, et al. Adipocyte death defines macrophage localization and function in adipose tissue of obese mice and humans. J Lipid Res 2005;46:2347–2355
12. Chavez JA, Summers SA. A ceramide-centric view of insulin resistance. Cell Metab 2012;15:585–594
13. Haus JM, Kashyap SR, Kasumov T, et al. Plasma ceramides are elevated in obese subjects with type 2 diabetes and correlate with the severity of insulin resistance. Diabetes 2009;58:337–343
14. Yamashita T, Hashiramoto A, Haluzik M, et al. Enhanced insulin sensitivity in mice lacking ganglioside GM3. Proc Natl Acad Sci U S A 2003; 100:3445–3449
15. Ulland TK, Colonna M. TREM2 - a key player in microglial biology and Alzheimer disease. Nat Rev Neurol 2018;14:667–675
16. Sharif O, Knapp S. From expression to signaling: roles of TREM-1 and TREM-2 in innate immunity and bacterial infection. Immunobiology 2008;213:701–713
17. Guerreiro R, Wojtas A, Bras J, et al.; Alzheimer Genetic Analysis Group. TREM2 variants in Alzheimer's disease. N Engl J Med 2013;368:117–127
18. Cannon JP, O'Driscoll M, Litman GW. Specific lipid recognition is a general feature of CD300 and TREM molecules. Immunogenetics 2012;64:39–47
19. Wang Y, Cella M, Mallinson K, et al. TREM2 lipid sensing sustains the microglial response in an Alzheimer's disease model. Cell 2015;160:1061–1071
20. Ulland TK, Song WM, Huang SCC, et al. TREM2 maintains microglial metabolic fitness in Alzheimer's disease. Cell 2017;170:649–663.e13
21. Park M, Yi JW, Kim EM, et al. Triggering receptor expressed on myeloid cells 2 (TREM2) promotes adipogenesis and diet-induced obesity. Diabetes 2015;64:117–127
22. Turnbull IR, Gilfillan S, Cella M, et al. Cutting edge: TREM-2 attenuates macrophage activation. J Immunol 2006;177:3520–3524
23. Jais A, Einwallner E, Sharif O, et al. Heme oxygenase-1 drives metaflammation and insulin resistance in mouse and man. Cell 2014;158:25–40
24. Saluzzo S, Gorki AD, Rana BMJ, et al. First-breath-induced type 2 pathways shape the lung immune environment. Cell Rep 2017;18:1893–1905
25. Galic S, Fullerton MD, Schertzer JD, et al. Hematopoietic AMPK β1 reduces mouse adipose tissue macrophage inflammation and insulin resistance in obesity. J Clin Invest 2011;121:4903–4915
26. Raichur S, Wang ST, Chan PW, et al. CerS2 haploinsufficiency inhibits β-oxidation and confers susceptibility to diet-induced steatohepatitis and insulin resistance [published correction appears in Cell Metab 2014;20:919]. Cell Metab 2014;20:687–695
27. Ussher JR, Koves TR, Cadete VJ, et al. Inhibition of de novo ceramide synthesis reverses diet-induced insulin resistance and enhances whole-body oxygen consumption. Diabetes 2010;59:2453–2464
28. Tran TT, Kahn CR. Transplantation of adipose tissue and stem cells: role in metabolism and disease. Nat Rev Endocrinol 2010;6:195–213
29. Tran TT, Yamamoto Y, Gesta S, Kahn CR. Beneficial effects of subcutaneous fat transplantation on metabolism. Cell Metab 2008;7:410–420
30. de la Monte SM, Wands JR. Alzheimer's disease is type 3 diabetes-evidence reviewed. J Diabetes Sci Technol 2008;2:1101–1113
31. Gonzalez FJ, Xie C, Jiang C. The role of hypoxia-inducible factors in metabolic diseases. Nat Rev Endocrinol 2018;15:21–32
32. Strissel KJ, Stancheva Z, Miyoshi H, et al. Adipocyte death, adipose tissue remodeling, and obesity complications. Diabetes 2007;56:2910–2918
33. Oh DY, Morinaga H, Talukdar S, Bae EJ, Olefsky JM. Increased macrophage migration into adipose tissue in obese mice. Diabetes 2012;61:346–354
34. Fujisaka S, Usui I, Bukhari A, et al. Regulatory mechanisms for adipose tissue M1 and M2 macrophages in diet-induced obese mice. Diabetes 2009; 58:2574–2582
35. Schooneman MG, Vaz FM, Houten SM, Soeters MR. Acylcarnitines: reflecting or inflicting insulin resistance? Diabetes 2013;62:1–8
36. Turpin SM, Nicholls HT, Willmes DM, et al. Obesity-induced CerS6-dependent C16:0 ceramide production promotes weight gain and glucose intolerance. Cell Metab 2014;20:678–686
37. Chaurasia B, Tippetts TS, Mayoral Monibas R, et al. Targeting a ceramide double bond improves insulin resistance and hepatic steatosis. Science 2019; 365:386–392
38. Stratford S, Hoehn KL, Liu F, Summers SA. Regulation of insulin action by ceramide: dual mechanisms linking ceramide accumulation to the inhibition of Akt/protein kinase B. J Biol Chem 2004;279:36608–36615
39. Turpin-Nolan SM, Hammerschmidt P, Chen W, et al. CerS1-derived $C_{18:0}$ ceramide in skeletal muscle promotes obesity-induced insulin resistance. Cell Rep 2019;26:1–10.e7
40. Sica A, Mantovani A. Macrophage plasticity and polarization: in vivo veritas. J Clin Invest 2012;122:787–795
41. Ito A, Suganami T, Yamauchi A, et al. Role of CC chemokine receptor 2 in bone marrow cells in the recruitment of macrophages into obese adipose tissue. J Biol Chem 2008;283:35715–35723
42. Holland WL, Miller RA, Wang ZV, et al. Receptor-mediated activation of ceramidase activity initiates the pleiotropic actions of adiponectin. Nat Med 2011;17:55–63
43. Takahashi K, Rochford CD, Neumann H. Clearance of apoptotic neurons without inflammation by microglial triggering receptor expressed on myeloid cells-2. J Exp Med 2005;201:647–657
44. Nawaz A, Aminuddin A, Kado T, et al. $CD206^+$ M2-like macrophages regulate systemic glucose metabolism by inhibiting proliferation of adipocyte progenitors. Nat Commun 2017;8:286
45. Xia JY, Holland WL, Kusminski CM, et al. Targeted induction of ceramide degradation leads to improved systemic metabolism and reduced hepatic steatosis. Cell Metab 2015;22:266–278
46. Chaurasia B, Kaddai VA, Lancaster GI, et al. Adipocyte ceramides regulate subcutaneous adipose browning, inflammation, and metabolism. Cell Metab 2016;24:820–834
47. Verloes A, Maquet P, Sadzot B, Vivario M, Thiry A, Franck G. Nasu-Hakola syndrome: polycystic lipomembranous osteodysplasia with sclerosing leucoencephalopathy and presenile dementia. J Med Genet 1997;34:753–757
48. Yokoi S, Suzuki K, Amano N, Yagishita S. Fatty acid analysis of galactolipids and ganglioside in the brains of four cases of Nasu-Hakola disease. Jpn J Psychiatry Neurol 1989;43:695–701